Magnetohydrodynamic flow and heat transfer around a heated cylinder of arbitrary conductivity

IOP Conf. Series: Journal of Physics: Conf. Series **923** (2017) 012024 doi:10.1088/1742-6596/923/1/012024

Magnetohydrodynamic flow and heat transfer around a heated cylinder of arbitrary conductivity

A Tassone, M Nobili and G Caruso

Department of Astronautical, Electrical and Energy Engineering-Nuclear Section, "Sapienza" University of Rome, Corso Vittorio Emanuele II, 244, 00186 Roma, Italy

E-mail: alessandro.tassone@uniroma1.it

Abstract. The interaction of the liquid metal with the plasma confinement magnetic field constitutes a challenge for the design of fusion reactor blankets, due to the arise of MHD effects: increased pressure drops, heat transfer suppression, etc. To overcome these issues, a dielectric fluid can be employed as coolant for the breeding zone. A typical configuration involves pipes transverse to the liquid metal flow direction. This numerical study is conducted to assess the influence of pipe conductivity on the MHD flow and heat transfer. The CFD code ANSYS CFX was employed for this purpose. The fluid is assumed to be bounded by rectangular walls with non-uniform thickness and subject to a skewed magnetic field with the main component aligned with the cylinder axis. The simulations were restricted to $Re = (20, 40)$ and $M = (10, 50)$. Three different scenarios for the obstacle were considered: perfectly insulating, finite conductivity and perfectly conducting. The electrical conductivity was found to affect the channel pressure penalty due to the obstacle insertion only for $M = 10$ and just for the two limiting cases. A general increment of the heat transfer with M was found due to the tendency of the magnetic field to equalize the flow rate between the sub-channels individuated by the pipe. The best results were obtained with the insulating pipe, due to the reduced electromagnetic drag. The generation of counter-rotating vortices close to the lateral duct walls was observed for $M = 50$ and perfectly conducting pipe as a result of the modified currents distribution.

1. Introduction

The flow of an electrically conductive fluid in the presence of an applied magnetic field deviates from the ordinary hydrodynamic behavior due to the arising of induced currents in the fluid bulk, which generate a volumetric Lorentz force that reduces the flow mean velocity and drastically modifies its features. Enhanced corrosion rates, turbulence suppression and additional pressure drops are some of the effects caused by the transition to a magnetohydrodynamic (MHD) flow regime [1][2].

MHD flows are of interest for many industrial applications, including the design of breeder blankets for nuclear fusion reactors [3]. Since the tritium breeder material is lithium, eutectic alloys like LiPb have been considered in the past for their excellent thermal properties as working fluids. To ensure the required cooling of the breeding zone, one of the strategies adopted is to insert pipes transverse to the main flow direction [4].

The bounded flow past a cyrcular cylinder is a classic case studied in hydrodynamics and recently it has been investigated in a MHD perspective. The blockage ratio (β) and the obstacle offset from the duct centerline (G/d) are the most important geometric parameters and, together

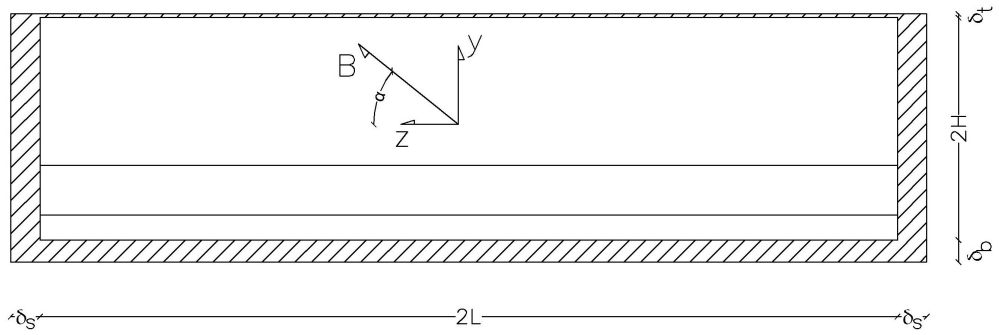

(a) Radial-poloidal cross-section

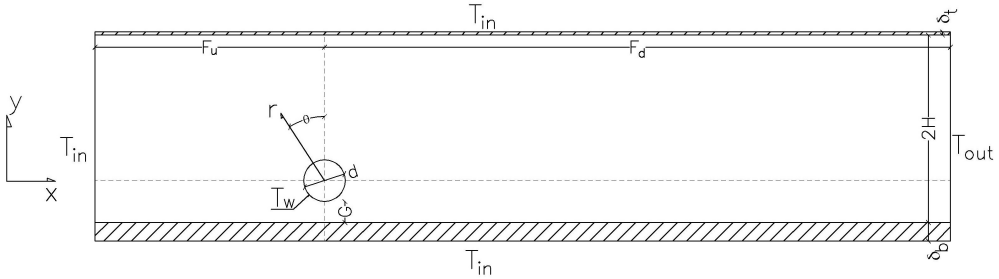

(b) Toroidal-poloidal cross-section

Figure 1: Problem geometry

with the magnetic field orientation respect to the main stream direction, define the flow. The particular case of magnetic field transverse to the flow but aligned to the obstacle axis has been extensively studied in recent years for its importance in fusion blanket engineering [5][6].

Tassone et al. [7] investigated the flow dynamics and heat transfer for the bounded MHD flow past an heated, electrically insulating, cylinder. Common features encountered in the most recent blanket designs, i.e. skewed magnetic field with the dominant component aligned with the obstacle axis and duct walls of non-uniform thickness, were considered [8]. This work aims to integrate those results by investigating the influence of the cylinder electrical conductivity on the flow pattern and heat transfer mechanisms.

2. Problem formulation

The geometry considered in this work is shown in Figure 1 and a complete overview of the problem geometrical parameters is available in Table 1. A rectangular duct accommodates the obstacle; it is defined by a toroidal half-length L and poloidal half-length H. The duct walls have non-uniform thickness (δ) and satisfy the thin-wall approximation ($\delta \ll L$). The cylinder is defined by blockage ratio $\beta = d/2H$ and offset from the duct centerline G/d, where G is the distance between the cylinder bottom and the closest duct wall. For finite conductivity simulations, inner diameter d_i and wall thickness δ_o were defined for the obstacle. The upstream and downstream lengths (F_u, F_d) identify the cylinder radial position in the duct.

The applied magnetic field $\mathbf{B} = (0, B_y, B_z)$ is uniform and constant in the channel region. The toroidal component is assumed to be dominant with the field inclination on the toroidal axis (α) being equal to 16°. The wall temperature of the external cylinder surface is assumed to be $T_w = 573\,K$. A constant temperature difference with the fluid at the channel inlet is considered such that $\Delta T = T_w - T_{in} = 30\,K$.

To model the behavior of a MHD flow, the Navier-Stokes equations must be combined with the Maxwell ones. The resulting set involves a non-linear and bidirectional coupling between the

Table 1: Test case geometry specifications

Duct par. [mm]		Cylinder par. [mm]		Wall thickness [mm]		Wall conductance $\times 10^2$	
L	117.00	d	13.500	δ_t	1.00	c_t	1.25
H	30.25	d_i	8.000	δ_b	6.00	c_b	7.50
F_u	74.25	G/d	0.500	δ_s	10.00	c_s	10.00
F_d	202.50	β	0.223	δ_o	2.75	c_o	$0 - 3.73 - \infty$

fluid velocity and the magnetic field. This phenomenon is mediated through the induced field, which is generated according to the Faraday's law of induction by the currents harbored inside the conductive fluid. A simplifying assumption, called the inductionless approximation, can be employed if the intensity of such field is negligible, thus to consider $\mathbf{B}$ as being determined only by the boundary conditions. This is accomplished if the magnetic Reynolds number $R_m = \mu\sigma u_0 L \ll 1$; where μ is the magnetic permeability, σ the electrical conductivity, u_0 and L velocity and length characteristic values [9].

Considering an incompressible fluid with constant thermophysical properties and a laminar inductionless MHD flow, the dimensionless governing equations can be derived as follows

$$\nabla \cdot \mathbf{u} = 0 \tag{1}$$

$$\frac{\partial \mathbf{u}}{\partial t} + (\mathbf{u} \cdot \nabla)\mathbf{u} = -\nabla p + \frac{1}{Re}\nabla^2 \mathbf{u} + N(\mathbf{J} \times \mathbf{B}) \tag{2}$$

$$\frac{\partial T}{\partial t} = (\mathbf{u} \cdot \nabla)T = \frac{1}{Pe}\nabla^2 T \tag{3}$$

$$\nabla^2 \phi = \nabla \cdot (\mathbf{u} \times \mathbf{B}) \tag{4}$$

Here, $\mathbf{u}, \mathbf{B}, \mathbf{J}, \phi, T$ and p represents the velocity, magnetic field, current density, electric potential, temperature and pressure scaled by the average inlet velocity u_0, the magnitude of the magnetic induction B_0, $j_0 = \sigma u_0 B_0$, $\phi_0 = d u_0 B_0$, the difference between the local temperature and T_{in} divided by ΔT and, finally, $p_0 = \rho u_0^2$. Lengths are scaled by the external cylinder diameter d, unless otherwise specified, which is also chosen as the length scale of the system for dimensionless parameters. An additional source term in (3) would be formally required to represent the Joule heating. However, in the formulation it has been neglected since it can be demonstrated that its influence for most liquid metal flows is negligible [5]. After solving the set (1-4), the Ohm's equation ($\mathbf{J} = -\nabla\phi + \mathbf{u} \times \mathbf{B}$) is employed to compute the current density from the electric potential distribution.

Reynolds (Re) and Péclet (Pe) numbers, together with the interaction parameter (N), appear in the governing equations and are defined as

$$Re = \frac{u_0 d}{\nu}, \qquad Pe = \frac{u_0 d}{\alpha_t}, \qquad N = \frac{M^2}{Re} \tag{5a,5b,5c}$$

where α_t is the thermal diffusivity. The Hartmann number (M) is a measure of the magnetic field intensity and, therefore, a fundamental MHD parameter

$$M = B_0 d \sqrt{\frac{\sigma}{\rho\nu}} \tag{6}$$

Table 2: Thermophysical properties of LiPb and Eurofer

	Lithium-Lead [10]	Eurofer97 [11]
ρ [kg m^{-3}]	$9.857 \cdot 10^3$	$7.695 \cdot 10^3$
σ [S m^{-1}]	$7.932 \cdot 10^5$	$1.259 \cdot 10^6$
k [W m^{-1} K^{-1}]	12.831	30.060
ν [m^2 s^{-1}]	$2.332 \cdot 10^{-7}$	n.a.
α_t [m^2 s^{-1}]	$6.885 \cdot 10^{-6}$	$7.193 \cdot 10^{-6}$

A fifth parameter, the wall conductance ratio (c), is needed to represent the influence of the electrical boundary conditions on the MHD flow features

$$c = \frac{\sigma_k}{\sigma}\frac{\delta_k}{L} \tag{7}$$

the quantities σ_k and δ_k refer to the wall electrical conductivity and thickness. Different thicknesses were considered for the duct walls, whose conductance ratios are reported in Table 1. The electrical conductivity of the obstacle material was changed each time to simulate insulating, conductive and perfectly conducting pipe.

A local Nusselt number is defined to assess the heat transfer between the obstacle and surrounding fluid employing the temperature gradient normal to the cylinder surface A

$$Nu_w = \frac{d}{T_w - T_{bulk}} \left.\frac{\partial T}{\partial r}\right|_A \tag{8}$$

the bulk temperature of the fluid is computed as the average value on a cylindrical surface S at $r = d$ from the center of the obstacle, weighted on the velocity distribution

$$T_{bulk} = \frac{\iint_S uT\, dS}{\iint_S u\, dS} \tag{9}$$

Accordingly, the average Nusselt number is obtained by

$$Nu = \frac{1}{A}\iint_A Nu_w\, dA \tag{10}$$

The pressure drop penalty due to the obstacle can be defined as the normalized difference between the measured drop and the one for the unperturbed channel (Δp_{2D}), calculated considering the pressure gradient at the outlet

$$p_o = \frac{\Delta p - \Delta p_{2D}}{\Delta p_{2D}} \tag{11}$$

3. Numerical strategy

The commercial CFD code ANSYS CFX 15 was employed to perform this study. The MHD model implemented in CFX relies on the inductionless approximation and, therefore, the governing equations outlined in section 2. The eutectic alloy LiPb was modeled with constant thermophysical properties evaluated at a reference temperature $T_{ref} = 558\,K$ (see Table 2). Correlations developed by Jauch et al. were employed for this purpose [10]. The resulting fluid is characterized by $Pr = 0.034$. The same treatment was applied to the solid domain, which was

modeled employing Eurofer97 steel according to the correlations outlined by Mergia & Boukos [11]. The only exception was constituted by the electrical conductivity that was modified to obtain the conductance ratio required to simulate different obstacles.

Typical velocities in the breeding zone for separate cooling fusion blanket ranges from 0.1 mm/s^{-1} to 5 mm/s^{-1} [4]. Accounting for the stabilizing effect of the magnetic field, the resulting low Reynolds number flow would be steady and laminar. For the purpose of this work, a range $Re = [20, 40]$ was considered. A constant mean velocity $u_0$was employed as initial condition for a 2D simulation that produced the fully developed flow velocity profile. This was assumed as the channel inlet BC, whereas at the outlet a zero pressure setting is specified. At the duct walls, no-slip BC for velocity is enforced. The range $Pe = [0.68, 1.36]$ for the Péclet number is derived from u_0 according to 5b.

Three scenarios were considered in the study according to the obstacle material: ideal dielectric, perfect conductor and Eurofer. For these test cases, simulations were performed for the specified Re range and for $M = [10, 50]$. Accompanying simulations for $M = 0$ were performed to highlight the difference with ordinary flows. Electrical boundary conditions must be specified to solve the MHD governing equations. On the duct external surfaces the normal current density flux is zero, as well as the electric potential gradient

$$\frac{\partial \phi}{\partial n} = 0 \tag{12}$$

Moreover, the BC (12) is employed on the cylinder surface to model the dielectric obstacle. For the duct walls and the finite conductivity obstacle, equation (4) must be solved to obtain the wall electric potential. This is accomplished by coupling the fluid and solid domain, assuming the potential and current density conservation at the interface

$$\phi = \phi_w, \qquad \mathbf{J_n} = \mathbf{J_{n,w}} \tag{13a,13b}$$

For the perfectly conducting obstacle, BCs (13a-13b) were also employed assuming $\sigma_o = \infty$. The obstacle/fluid interface is assumed at a fixed temperature $T_w = 573\,K$, as well as the inlet, where $T_{in} = 543\,K$. The solid domain external surfaces are adiabatic.

A preliminary study was performed to ensure the result independence from the grid resolution. Simulations were carried out for the insulating obstacle case at $Re = 20$ and $M = 10$ employing five meshes with increasing number of nodes on the cylinder circumference and along the radial direction, ranging from $5 \cdot 10^5$ to $4 \cdot 10^6$ elements. A maximum 2% result divergence for the meshes considered was found [7].

4. Results and discussion

The flow transition from hydrodynamic to MHD behavior is described by the velocity contours presented in Figure 2. For the fully developed flow, the Lorentz force $\mathbf{F_L} = \mathbf{J} \times \mathbf{B}$ opposes the fluid movement and thus balances the driving pressure gradient in the duct center. The viscous forces are confined in thin boundary layers close to the walls that, depending on the relative orientation with the magnetic field, can have thickness $\delta \propto M^{-1}$ (perpendicular, *Hartmann layer*) or $\delta \propto M^{-1/2}$ (parallel, *Shercliff layer*). Since in the present study no wall is perfectly aligned with the magnetic field ($\alpha \gg M^{-1/2}$), the Hartmann layer behavior is observed throughout the duct [12]. Moreover, an internal layer parallel to the magnetic field lines is formed across the core in fully developed condition. This feature carries the bulk of the flow rate and connects two opposite duct corners where high velocity jets are located. This structure formation can be explained by the detachment of the Shercliff layer jets, which would be present for a toroidal magnetic field at $y/H = \pm 1$, from the associated walls and its smearing over the core. The top jet is promoted thanks to the nearby low conductivity wall: those currents whose

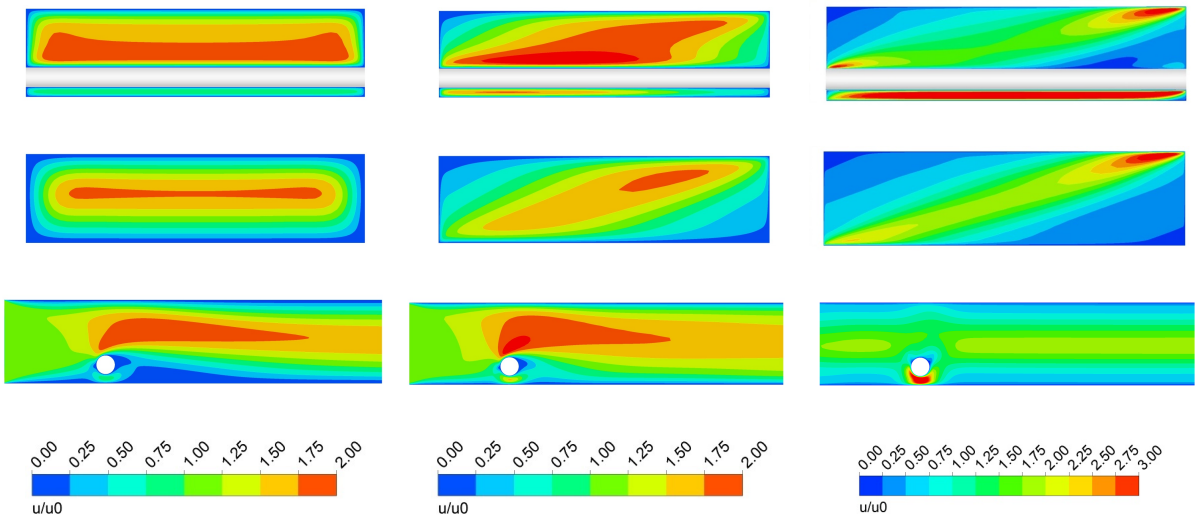

(a) $M = 0$ (b) $M = 10$ (c) $M = 50$

Figure 2: Velocity contour comparison for $Re = 20$. Top and middle row: toroidal-poloidal view at cylinder center ($x/d = 0$) and $x/d = 10$; bottom row: poloidal-radial view at $z/L = 0$. Note that the velocity scale for $M = 50$ covers an higher range. The cylinder is perfectly insulating ($c_o = 0$).

close their path through this wall have a reduced intensity and, therefore, generate a decreased electromagnetic drag. The reversed phenomenon is experienced by the bottom jet [13].

The cylinder offset breaks the duct symmetry in two sub-channels of uneven cross-section, thus the lower, smaller, channel offers a greater hydraulic resistance and carries just $6 - 9\%$ of the total mass flow rate in the hydrodynamic case for Re considered. Increasing M, a stream shift to this channel is observed and, for $M = 50$, its flow rate increases to $\simeq 28\%$ of the total. This phenomenon can be explained by the electromagnetic drag introduction in the duct that, even for low M, it is dominant over the hydraulic losses and it is larger for the top channel due to the lower resistivity experienced by the currents closing through it.Moreover, the sub-channels are linked by the lateral walls and such phenomenon allows currents to pass through both, electrically coupling them, and further compensating the flow rate imbalance [2]. The magnetic field extends the range of stability of the creeping flow regime, which is found for all the cases considered except $M = 10, Re = 40$, where, however, the steady vortices observed in the cylinder wake are partially suppressed [7].

For a fully developed flow, the induced currents are confined to a plane perpendicular to the main flow direction and the flow is essentially 2D [9]. Introducing the obstacle creates velocity gradients in both the radial and poloidal direction thus, from (4), potential differences. The appearance of radial currents is observed, together with a pressure drop increase, and the MHD flow becomes 3D.

The obstacle pressure drop penalty (p_o) is influenced mainly by the flow mean velocity u_0 and the magnetic field intensity B_0, which both appear in the fully developed pressure gradient expression ($dp/dx \propto \sigma u_0 B^2$). The 3D pressure drop term is as well function of these parameters and influenced by the geometrical features of the model, as such β and G/d [5]. However, this component usually features a weaker dependence on B_0 compared with the 2D one, which means that, for constant Re, the increase in M reduces the pressure drop penalty because $\Delta p \backsimeq \Delta p_{2D}$. Keeping M constant instead, the pressure penalty increases with Re but, for $M \to \infty$, this increment becomes negligible [7].

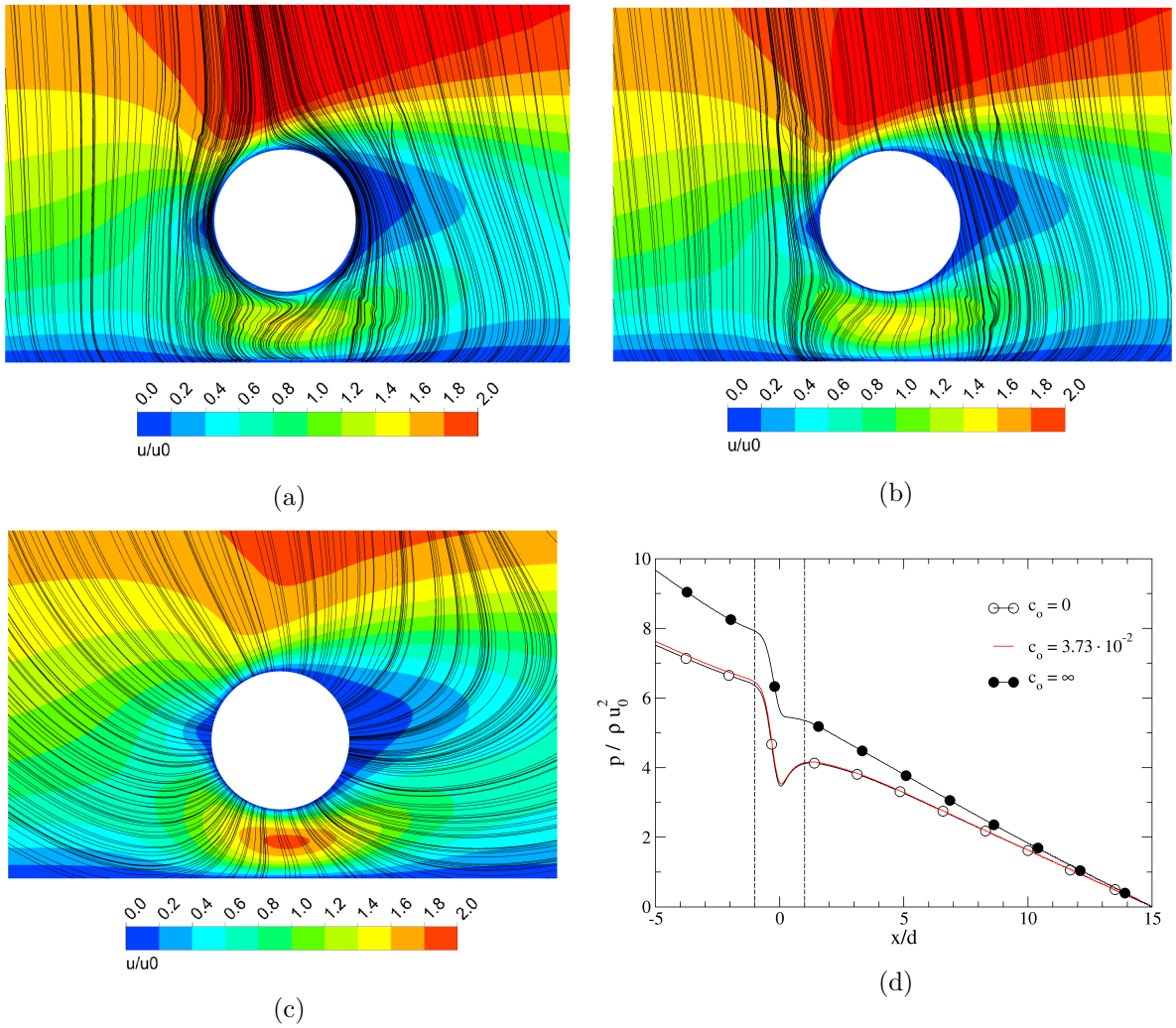

Figure 3: Influence of obstacle conductivity on current path in the fluid domain and channel pressure drop: a) $c_o = 0$, b) $c_o = 3.73$, c) $c_o = \infty$, d) pressure profile along the radial line at $z, y = 0$. Test case $M = 10, Re = 20$. Dotted lines in Figure 3d mark cylinder position.

The obstacle conductivity influences the current paths in the surrounding area in turn affecting the flow pattern and the heat transfer. In Figure 3a, the perfectly insulating surface of the cylinder forbids the currents to penetrate inside the obstacle, forcing them to close through the thin Hartmann layers. It can be observed that the path perturbation introduced by the obstacle extends farther downstream than the wake, which is quickly suppressed by the magnetic field. Conversely, a conductive surface offers a less resistant path than the boundary layer for the currents that, therefore, will tend to close through the cylinder wall. In Figure 3b, this behavior is marked by the streamlines skipping through the boundary layer to enter the solid domain (not represented) and being "attracted" by the obstacle. This phenomenon is evident in Figure 3c where passing through the perfectly conducting cylinder is so favorable that all the currents generated, both upstream and downstream, are collected by the obstacle. This current distribution tends to push away the flow from the duct center toward the poloidal wall at $z/L = -1$ for the top sub-channel and the wall at $z/L = 1$ for the bottom one. For $c_o = \infty$, a slight increase in the channel pressure drop is observed due to these phenomena, whereas for the

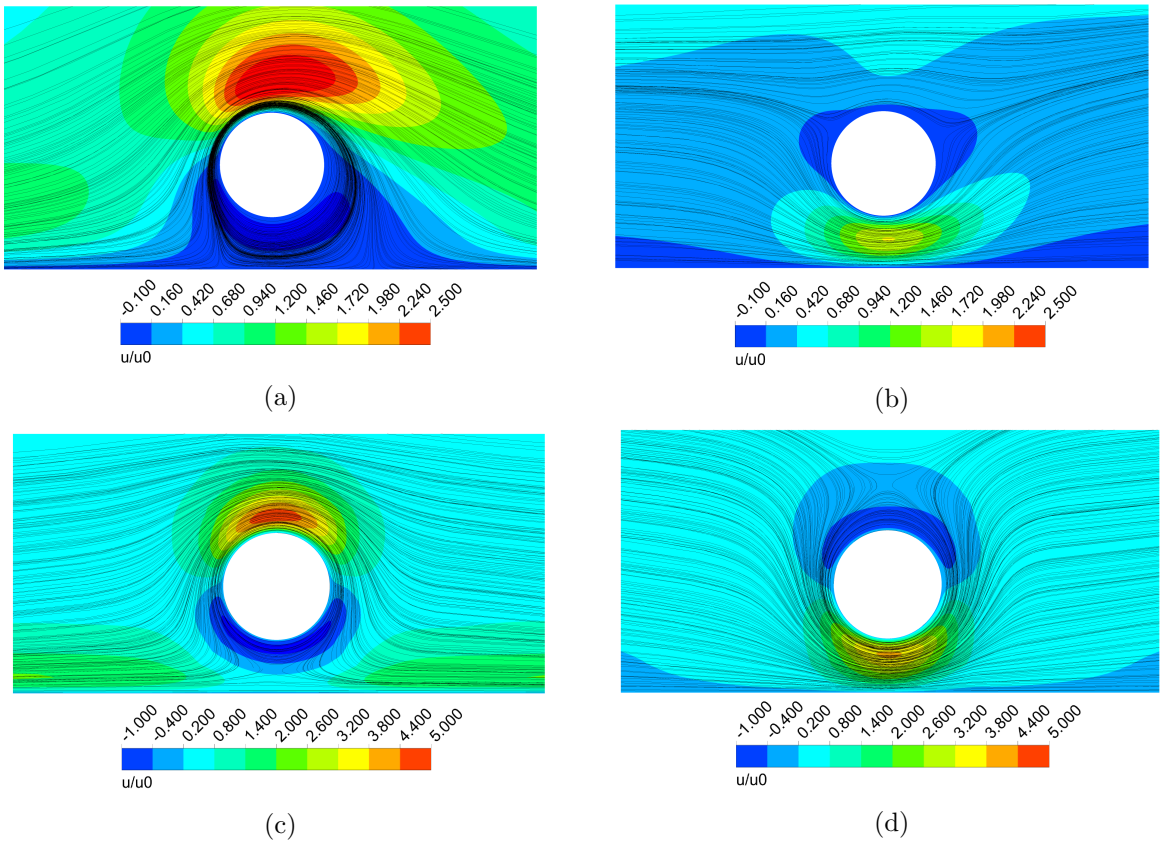

Figure 4: Near-wall vortex formation for perfectly conducting obstacle ($c_o = \infty$) and $Re = 20$. Left: streamline and dimensionless velocity contour at $z/L = -0.95$ and; right: at $z/L = 0.95$. Top row: results at $M = 10$ and; bottom row: at $M = 50$.

intermediate value the obstacle influence on the current distribution is not significant enough to observe a deviation from the insulating case (see Figure 3d). This behavior is mirrored by an increase in the pressure penalty, which for $M = 10$ reaches 40%. Conversely, no significant effect on the pressure penalty is found for $M = 50$ (see Table 3).

Another interesting feature of the $c_o = \infty$ case is the formation of near-wall counter-rotating vortices around the obstacle and close to the poloidal walls. In Figure 4, it can be seen how for $M = 10$ the high velocity jet localized close to the wall at $z/L = -1$ in the top sub-channel is accompanied by a slow, clockwise rotating, vortex that spans across the height of the bottom sub-channel. The vortex is formed by the same localized electromagnetic drag that shifts the bottom jet to the wall at $z/L = 1$. Close to the opposite wall, the flow in the top sub-channel is suppressed but the braking force is not strong enough to provoke a flow inversion. This can be explained by the involved currents in the top sub-channel closing through a longer (thus more resistive) path in the liquid metal. Instead, for the $M = 50$ case the Lorentz forces are strong enough to trigger the counter-clockwise vortex. Due to the angular momentum conservation and the jet peak velocity being proportional to the magnetic field intensity, the vortices shrink closer to the obstacle for increasing M.

The effect of the obstacle conductivity on the heat transfer is less dramatic than on flow dynamics and it is found to lose importance with the increase of the intensity of the applied magnetic field. For $M = 10$ and $c = \infty$, the flow pattern modifications sustain an increase $\Delta Nu = +3.1\%$ compared with the $c = 0$ case for $Re = 20$. This increment can be ascribed

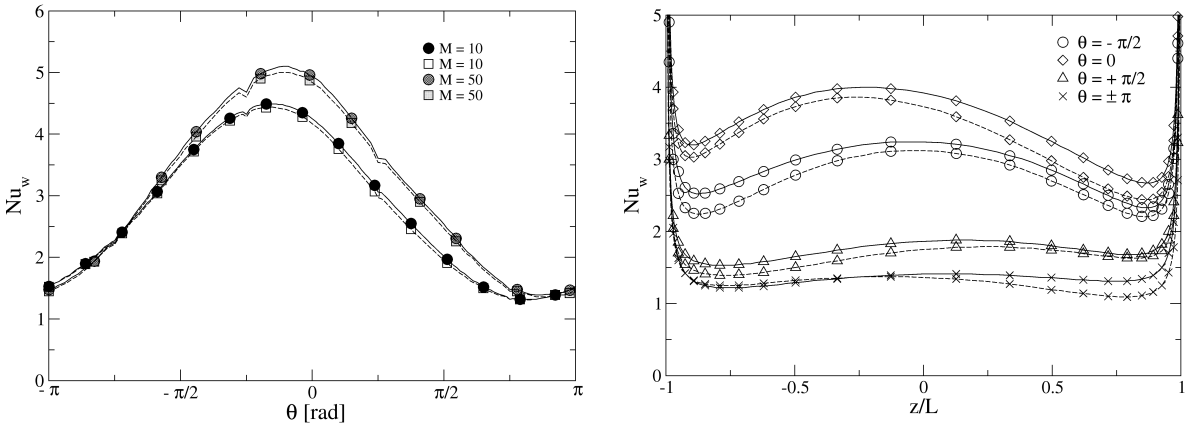

(a) (b)

Figure 5: Influence of obstacle conductivity on local Nusselt number: a) plot along cylinder outer circumference at $z/L = 0$ for increasing M, b) plots along lines parallel to cylinder axis for four relevant azimuthal coordinates (top: $-\pi/2$), front: 0, bottom: $\pi/2$, back: $\pm\pi$) at $Re = 20$. Solid and dotted lines refer respectively to $c = \infty$ and $c = 0$.

Table 3: Pressure penalty and average Nusselt number for different obstacle conductivity. The label E stands for the Eurofer case ($c_o = 3.73 \cdot 10^{-2}$).

	M		10			50	
	c	0	E	∞	0	E	∞
p_o [%]	$Re = 20$	14.074	15.377	34.975	10.918	11.319	12.683
	$Re = 40$	21.128	22.105	40.741	13.356	10.686	14.613
Nu	$Re = 20$	2.5549	2.5427	2.6340	3.1440	3.1325	3.1513
	$Re = 40$	2.6019	2.6046	2.6634	3.1502	3.0893	3.1219

to higher peak velocity for the obstacle jets (compensating for the additional drag in the core) and mass flow rate in the bottom sub-channel (see Figure 5). For $Re = 40$, a similar behavior is observed with a smaller difference between the limiting cases ($\Delta Nu = +2.4\%$). The finite conductivity test case was found to have slightly worse or equal Nu compared with $c_o = 0$. For $M = 50$, the mass flow rate carried by the bottom sub-channel increases from $\sim 10\%$ to $\sim 25\%$ in the Re range considered and the Nusselt number rises accordingly for all the simulations [7]. However, the insulating cylinder is found to perform better compared with the conductive one due to the reduced electromagnetic drag experienced by the fluid. For $c = \infty$, the near-wall vortices sustain the heat transfer bringing the Nu even on par with the insulating case at $Re = 20$ and limiting the net loss at $\Delta Nu = -0.9\%$ for $Re = 40$.

5. Conclusions

The influence of obstacle conductivity on flow dynamics and heat transfer for a bounded MHD flow past a heated cylinder was investigated. Three cases for the obstacle wall conductance ratio (c_o) were considered: perfectly insulating ($c_o = 0$), finite conductivity and perfectly conducting ($c_o = \infty$). The considered range of the Re number was low enough to allow the performing of only steady-state simulations. However, due to the complex magnetic field topology and the

List of symbols

B	magnetic induction [T]	α	magnetic field inclination [°]
d/d_i	outer/inner cyl. diameter [m]	α_t	thermal diffusivity [m^2/s]
H	poloidal half-length [m]	β	blockage ratio
J	current density [A/m^2]	δ	wall thickness [m]
L	toroidal half-length [m]	κ	thermal conductivity [W/mK]
p	pressure [Pa]	μ	magnetic permeability [H/m]
T	temperature [K]	ν	kinematic viscosity [m^2/s]
u	velocity [m/s]	ρ	density [kg/m^3]
r, θ, z	cylindrical coordinate system	σ	electrical conductivity [S/m]
x, y, z	radial, poloidal, toroidal axis	ϕ	electric potential [V]
G/d	offset from centerline	c	wall conductance ratio
M	Hartmann number	N	interaction parameter
Re	Reynolds number	R_m	magnetic Reynolds number
Pe	Péclet number	Pr	Prandtl number
p_o	obstacle pressure penalty [%]	Nu	average Nusselt number

non-uniform wall conductance ratio for the bounding walls, a full 3D computational domain, constituted of solid and fluid bodies, was required to solve the MHD governing equations. Two Hartmann numbers ($M = 10, 50$) were considered.

For low M, the pressure penalty was found to increase with c_o since the obstacle acts like a magnet on the current streamlines, triggering the arise of stronger 3D MHD effects that results in heavier pressure drops. Since the pressure gradient due to the 2D flow is proportional to B_0^2, this effect loses importance for an increasing M and already at $M = 50$ is negligible. No significant difference was found regarding the total pressure drop between the insulating and finite conductivity case.

The influence on the flow dynamics exerted by the modified Lorentz force distribution is significant for the $c_o = \infty$ case. The main feature is the generation of two counter-rotating vortices close to the poloidal walls at $M = 50$. These structures seem to have little repercussion on the overall flow behavior all but buffering the heat transfer losses due to the higher electromagnetic drag. The perfectly conducting case is found to perform slightly better than the finite conductivity scenario in these conditions, even though inferior to the insulating one.

References

[1] Kirillov I R, Reed C B, Barleon L and Miyazaki K 1995 *Fusion Eng. Des.* **27** 553–569
[2] Smolentsev S *et al.* 2010 *Fusion Eng. Des.* **85** 1196–1205
[3] Abdou M *et al.* 2015 *Fusion Eng. Des.* **100** 2–43
[4] Del Nevo A, Martelli E, Agostini P, Arena P, Bongiovì G, Caruso G, Di Gironimo G, Di Maio P, Eboli M, Giammusso R *et al.* 2017 *Fusion Eng. Des.*
[5] Hussam W K and Sheard G J 2013 *Int. J. Heat Mass Transf.* **67** 944–954
[6] Dousset V 2009 *Numerical simulations of MHD flows past obstacles in a duct under externally applied magnetic field* Ph.D. thesis Coventry University
[7] Tassone A, Nobili M and Caruso G 2017 *Proc. of CHT-17 7th Int. Symp. on Adv. in Comp. Heat Transfer* (in pubblication)
[8] Tassone A, Caruso G, Del Nevo A and Di Piazza I 2017 *Fusion Eng. Des.* (in pubblication)
[9] Müller U and Bühler L 2013 *Magnetofluiddynamics in channels and containers* (Springer Science & Business Media)
[10] Jauch U, Karcher V, Schulz B and Haase G 1986 *Thermophysical properties in the system Li-Pb*
[11] Mergia K and Boukos N 2008 *J. Nucl. Mater.* **373** 1–8
[12] Shercliff J 1981 *Zeitschrift für Angewandte Math. und Physik (ZAMP)* **32** 546–554
[13] Tao Z and Ni M 2015 *Sci. China Physics, Mech. & Astron.* **58** 1–18